ELSEVIER

Sedimentary Geology 119 (1998) 311–335

Sedimentary Geology

Diagenesis of shallowly buried cratonic sandstones, southwest Sinai, Egypt

Alaa M.K. Salem [a], Antar Abdel-Wahab [a], Earle F. McBride [b,*]

[a] *Department of Geology, Faculty of Education at Kafr El-Sheikh, Tanta University, Kafr El-Sheikh, Egypt*
[b] *Department of Geological Sciences, University of Texas at Austin, Austin, TX 78712, USA*

Received 14 July 1997; accepted 12 March 1998

Abstract

In spite of their age, quartzose and feldspathic Lower Carboniferous sandstones deposited on the Arabian shield in western Sinai remain friable and porous (average of 19%, maximum of 25%) except for strongly cemented ferricretes and silcretes. These fluvial and shallow-marine sandstones were not buried more than 1.5 km until Late Cretaceous and younger time, when the deepest rocks reached 2.5 km. Owing to shallow burial depths and episodic exposure, meteoric water dominated the pore system for most of geologic time: iron oxides had multiple diagenetic stages and yield Carboniferous and Late Cretaceous paleomagnetic signatures, and oxygen isotopic data for authigenic quartz, sparry calcite, and kaolinite yield meteoric signatures. The most significant diagenetic changes were: (1) cementation by iron oxide that locally reaches 40% in groundwater ferricretes; (2) reduction in porosity to 19% from an assumed original porosity 45% (19% porosity was lost by compaction and 7% by cementation); (3) generation of diagenetic quartzarenites by the loss of 7% detrital feldspar by kaolinization and dissolution; and (4) development of three thin mature silcretes apparently by thermal groundwaters. Some outcrop samples have halite and gypsum cements of young but uncertain origin: recycled from topographically higher younger rocks or from aerosols? Mature silcretes are strongly cemented by microcrystalline quartz, multiply zoned syntaxial quartz, and, originally, minor opal. Quartz overgrowths in most sandstones average only 2.2%, but display a variety of textures and in places overprint isopachous opal (now dissolved) grain coats. These features have more in common with incipient silcrete cement than normal burial quartz cement. Most silica was imported in groundwater.

Keywords: sandstone; diagenesis; meteoric water; ferricrete; silcrete; shallow burial

1. Introduction

Paleozoic sandstones, owing to their depth of burial and age, generally have low porosity owing to extensive compaction and cementation by quartz, calcite, and clay minerals (Table 1). We studied Carboniferous sandstones that were deposited on the Arabian shield in southwest Sinai, Egypt, that contrast markedly with the above norm. The sandstones from the Sinai are characterized by their friability, the presence of megapores that average 19% and which reach 25%, the dominance of iron oxides over quartz and calcite cements, and the localization of strong quartz cement in three mature silcretes. These shallow-marine and fluvial Carboniferous sandstones

* Corresponding author. Tel.: +1 (512) 471-1905; Fax: +1 (512) 471-9425; E-mail: efmcbride@mail.utexas.edu

0037-0738/98/$19.00
PII S0037-0738(98)00056-6

Table 1
Characteristics of some Carboniferous sandstones

Location	Max. burial depth (m)	ϕ (max., *mean*) %	Meteoric water input	Main authigenic minerals	Reference
Fort Worth basin, USA	2000	0	No	Q, C	McBride and Kimberly, 1963
North German basin	1800–5000	10	n.d.	Q, K	Füchtbauer, 1974
Anadarko basin, USA	2300	14 *5*	Yes	C, Q, I	Dutton and Land, 1985
Wyoming, USA	3200	23 *9*	Yes	Q, A, D	James, 1992
Val Verde basin, USA	n.d.	9	No	C, Q	Dutton et al., 1993
North China and Chitong basins	n.d.	n.d.	Yes	I, Q, C	Deng et al., 1996
S. Australia	n.d.	12	n.d.	Q, K, I	Hamlin et al., 1996
Arkoma basin, USA	7000	24	No	C, Ch, C	Spotl et al., 1996
Illinois basin, USA	2500?	∼15	Yes	Q, S, C	Hansely, 1996
Cooper basin, Australia	n.d.	n.d.	No	Q	Rezaee and Tingate, 1997
Sinai, Arabian shield	2300	25 *19*	Multiple	Fe (Q, K)	This study

Q: quartz; C: carbonate; D: dolomite; A: anhydrite; I: illite; K: kaolinite; Ch: chlorite; S: siderite; n.d.: no data; ∼: estimated from photomicrographs.

were buried less than 1.5 km for most of their history and are dominated by authigenic phases that formed in meteoric water. Thus, this study provides a case history of shallow-burial diagenesis in sandstones from a craton that was relatively stable and high-standing until Miocene and younger rifting (Purser et al., 1993).

The sandstones we studied are exposed in southwest Sinai marginal to the Gulf of Suez (Fig. 1). Here Precambrian and Paleozoic rocks are exposed in an eastward-dipping fault block that brings these old rocks adjacent to Cretaceous and Eocene rocks along a fault with 2000 m of displacement (Shata, 1956). The region also underwent minor folding in the late Paleozoic (Abdallah et al., 1992) and then rifting of the Gulf of Suez, which began in the early Miocene and continues to the present (Purser et al., 1993).

The rocks studied are composed mainly of sandstones with thin interbeds of shales, sandy shales and siltstones. There is also a 15-m thick unit of limestone-dolomite (Um-Bogma Formation; not studied) and black to green shales intercalated with these sandstones (Abu-Durba Formation; Fig. 2). The sandstones of interest to this study are exposed in a west-facing slope along a ridge nearly 100 km long. Stratigraphic sections were measured and sampled at three localities: Um Bogma (UB), Gebel Abu Durba (AD), and Gebel Naqus (N) (Figs. 1 and 3).

The age and stratigraphic subdivisions of the clastic formations in this area have been widely debated (summary in Salem, 1995, and Ibrahim, 1996). The Araba, Naqus, Sarabit, El-Khadim, Abu Hamata, Nasib, and Adedia formations have been considered as of Cambrian age by many authors based on their position on basement and the presence locally of *Scolithus* and stromatolites. However, a Carboniferous age for the Araba and Naqus formations has been advocated by some workers. Eames (1984) recovered Early Carboniferous palynomorphs from subsurface samples from the Gulf of Suez that are considered to be the Araba and Naqus formations. Ibrahim (1996) supports this age designation, but notes that the correlation between subsurface and surface units is not well documented. Confusing the issue are paleomagnetic data from two Araba/Naqus sandstone samples cemented by iron oxide that we collected and that yield signatures which fit Middle Cambrian pole positions. However, we accept, with reservations, the Early Carboniferous age advocated by Eames (1984) and Ibrahim (1996) because the diagenetic history of the age-disputed sandstones we studied is the same as that of the well-documented Carboniferous formations.

For the AD and N localities we accept the stratigraphic nomenclature of Klitzsch (1990) and his late Early Carboniferous age designation for the Um Bogma and Abu Thora formations (Fig. 2). For the Um Bogma succession we follow Weissbrod (1980), who divided the lower Paleozoic into four newly named formations, and the Abu Thora into two unnamed members (Fig. 2). Although correlation of

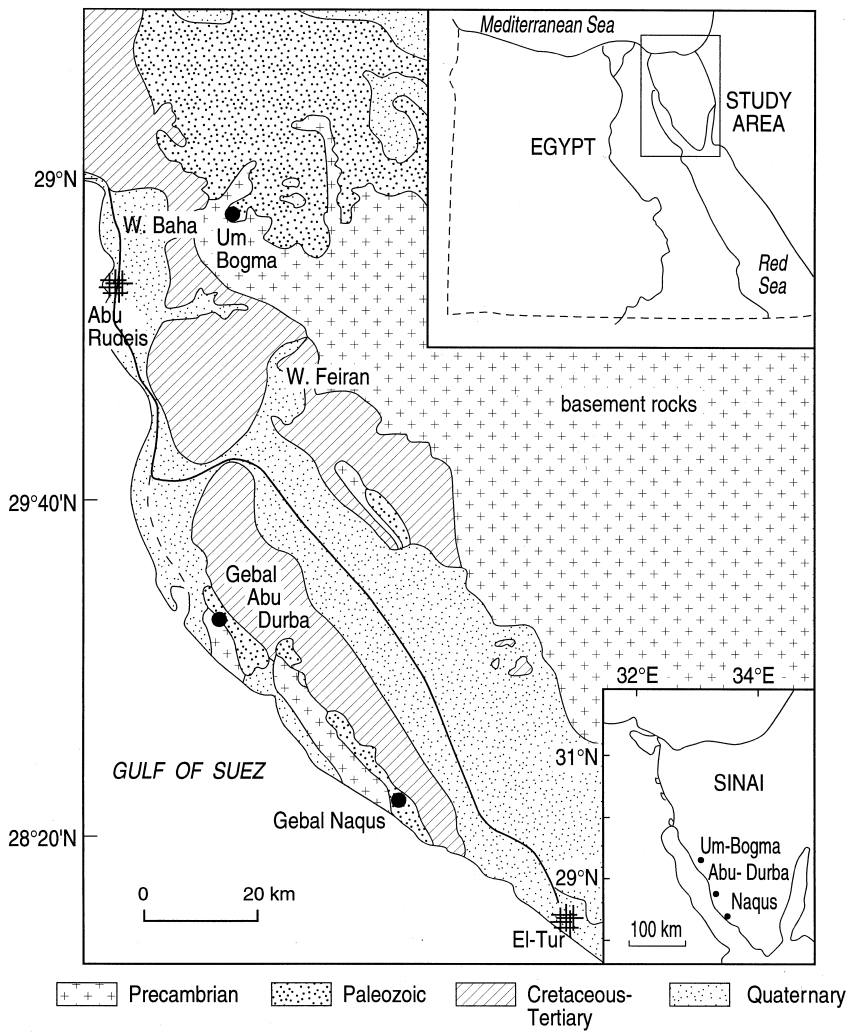

Fig. 1. Location map (after Eyal et al., 1980). Dots are sites of measured and sampled sections.

these old rocks between the UB and AD areas has not been established, we consider the four oldest formations at UB to be correlative with the Araba and Naqus formations and, thus, probably Carboniferous also. In this report we refer to the Araba, Naqus, Sarabit, El-Khadim, Abu Hamata, Nasib, and Adedia as older formations and the Abu Durba, Abu Thora and Um Bogma formations as younger formations.

The Paleozoic rocks in the study area are 90% sandstone and 10% siltstone and shale, although there is a thin manganiferous limestone and dolomite unit at the UB locality (Mart and Sass, 1972; Fig. 3). Colors of the sandstones are mostly brown or white; some are red or yellow. White sandstones lack iron oxide cement, whereas colored sandstones are pigmented by iron oxide. Some colored beds have a uniform color, others have iron oxide Liesegang bands, color mottling, isolated iron-oxide concretions or crusts. The rocks are 80% fluvial and 20% marine, but include 20 m of eolian dune deposits. Shales have yielded a few body fossils, but the sandstones have only trace fossils and rare stromatolites. Schematic logs of each measured section and sampling positions are given in Fig. 3. Details of stratigraphy and sedimentology of the rocks are given by Weissbrod (1969), Abdel-Wahab et al. (1987, 1992), Allam

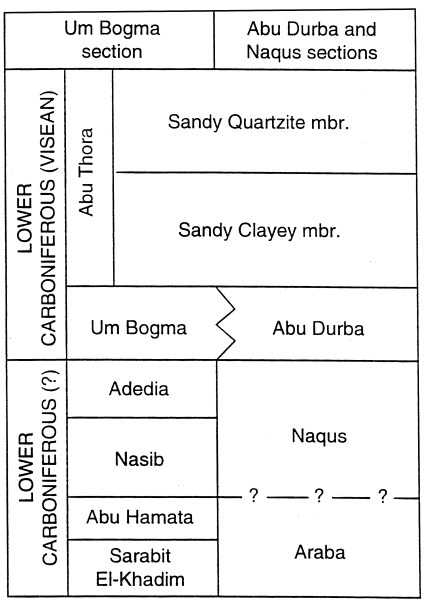

Fig. 2. Stratigraphic units included in this study.

(1989), Abdel-Wahab (1990) and Abdel-Wahab and McBride (1991). Ibrahim (1996) studied the petrography and diagenesis of the Naqus Formation from cores taken to depths of 3 km to 4 km beneath the Gulf of Suez. Abdel-Wahab and coworkers, cited above, also reported on diagenetic studies from this area. The thickness of the formations where we sampled them (~500 m) is typical of the region.

2. Procedure

Three stratigraphic sections with continuous exposure were measured and sampled. Thin sections were examined of 120 samples that were impregnated with blue-dyed epoxy resin. Many samples were stained for either K-feldspar using sodium cobaltinitrite or for calcite using alizarin Red-S. Four hundred counts per thin section were made of 100 samples to quantify the abundance of detrital grains, authigenic minerals, and pore abundance and types. Grain size and sorting were determined by measuring the maximum diameter of 30 random grains under the microscope.

Detrital and authigenic minerals were identified using a combination of thin sections, X-ray diffraction, scanning electron microscopy, cold cathode and scanned cathodoluminescence, and electron microprobe analysis. The carbon, oxygen, and strontium isotopic signature of selected samples of authigenic calcite were determined to aid in interpreting the temperature and diagenetic conditions of precipitation of this mineral phase, and the oxygen isotopic signature of authigenic quartz and kaolinite were determined to help determine the conditions of precipitation of these phases.

Fourteen sandstone samples with varying amounts of quartz overgrowths were analyzed to determine the oxygen isotopic composition of quartz cement using the technique of Land (1984). The isotopic composition of authigenic kaolinite was determined using the technique of Lynch (1994).

3. Burial history

The burial history (total subsidence) of these rocks is inferred from the thickness (uncorrected for compaction) and age of overlying rocks (Fig. 4). Uncertainties exist about the amount of uplift and thickness of rock removed by post-Cretaceous and post-Miocene erosion. The base of the Araba Formation at Um Bogma was buried almost to 2.5 km by the end of the Eocene epoch, but probably was not deeper than 1 or 1.5 km prior to Cretaceous time. Thus, the sandstones were buried less than ~1.5 km for nearly 200 Ma. Burial curves for the other localities are similar to that for the UB locality.

The thermal history is poorly known. The Sinai region migrated from approximately 35° southern latitude during the Carboniferous to the Equator by Cretaceous time (Paleomap, 1992). We assume that during much of this time the surface temperature was 20–25°C and the geothermal gradient was 25°C/km. Thus, the base of the Araba and time equivalent rocks probably did not reach a temperature in excess of 65° and possibly not in excess of 50° until after Cretaceous time (Fig. 4). A basalt sill of Late Triassic–Early Jurassic age (Weissbrod, 1969) at locality AD is the only evidence of Phanerozoic igneous activity in the study area that may have perturbed the burial thermal history. A more detailed analysis of the thermal history is given by Salem (1995).

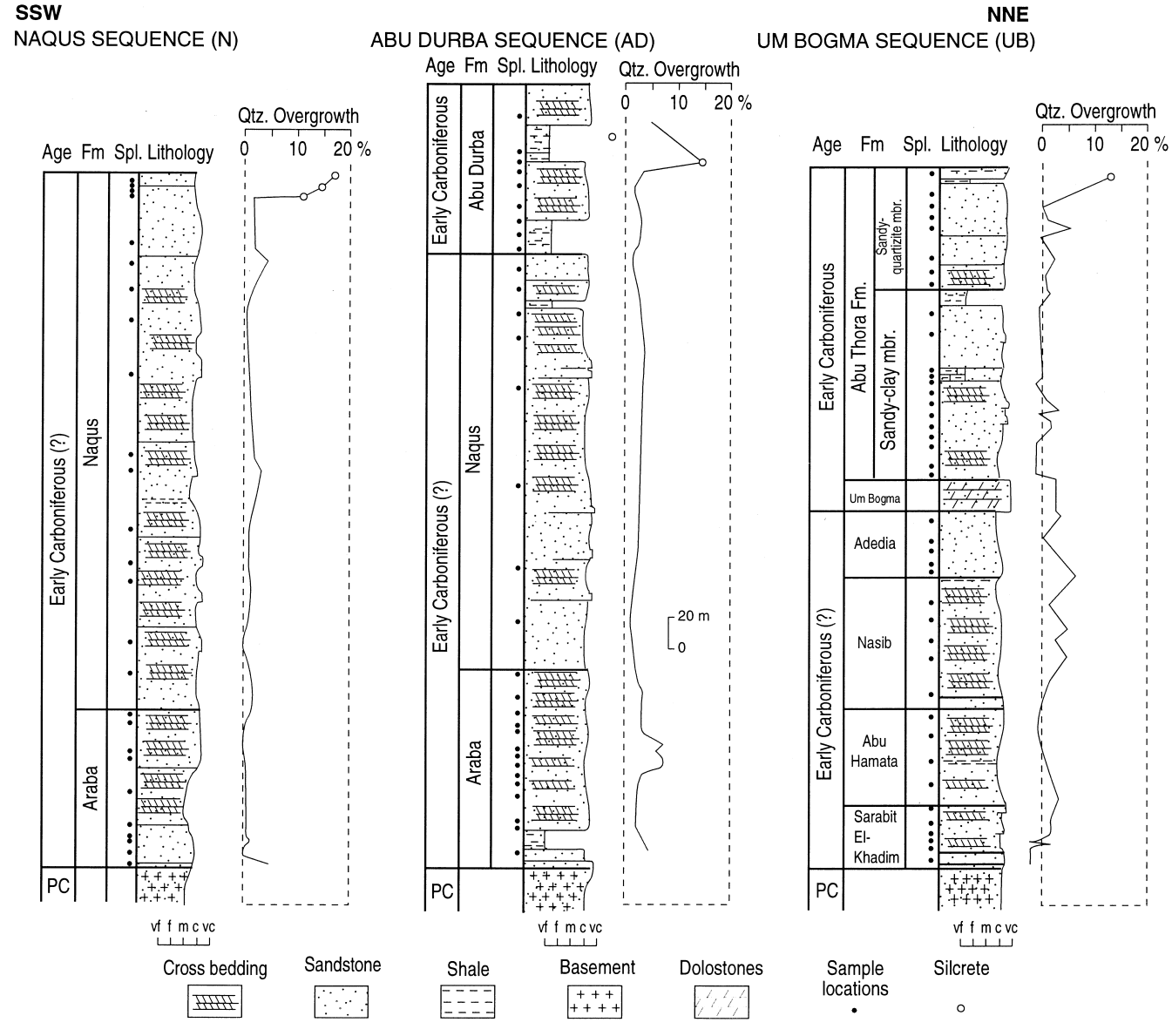

Fig. 3. Schematic stratigraphic sequence of three localities. Dots show sample sites. The lines show the amount of quartz cement in samples; mature silcrete samples are shown by open circles on the quartz cement curve.

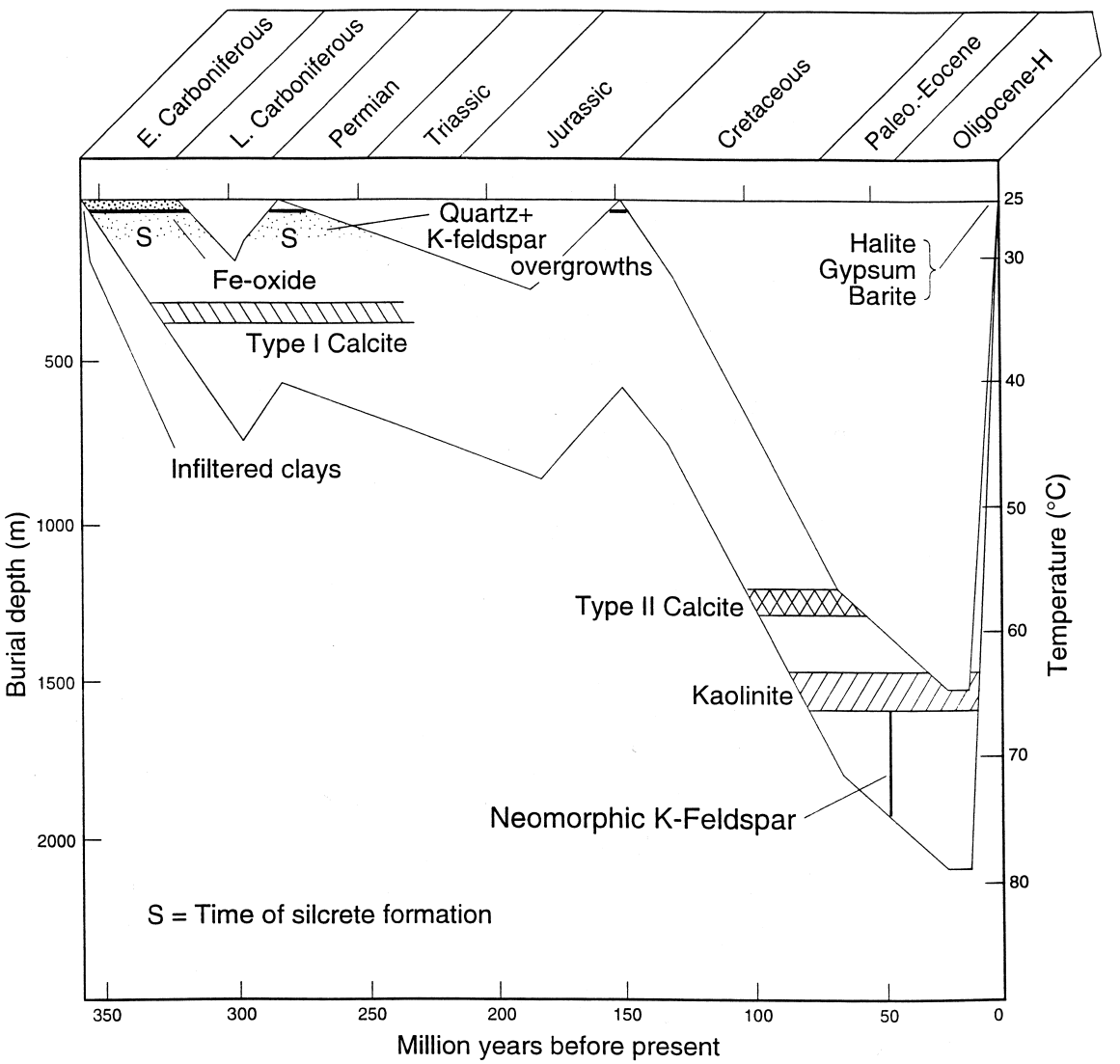

Fig. 4. Inferred burial and thermal history of rocks at the UB locality. Burial depth is the average thicknesses of overlying strata (Said, 1962); the thickness of rocks lost to erosion is estimated. Time of formation of major diagenetic events are also shown. The pre-Cretaceous time of silcrete formation is unknown, but *S* indicates inferred times of formation.

4. Texture and composition

The various formations are remarkably similar in texture and mineral composition and diagenetic character except that the older formations (Araba, Naqus, Sarabit, El-Khadim, Abu Hamata, Nasib, and Adedia) contain more feldspar (average of 9.3% in older sandstones and 0.2% in younger sandstones) and authigenic kaolinite (average of 6% in older and 0.2% in younger formations). Older sandstones have an average composition of 65% framework grains, 17% cement, and 18% porosity; younger sandstones average $F_{68}C_{13}P_{19}$. Primary detrital matrix is essentially absent from the sandstones, although unfiltered clay is present in some samples. Sandstones in the Naqus, Araba, Adedia, and Abu Thora formations today are quartzarenites; samples from the lower three formations at UB are subarkoses to arkoses. Rock frag-

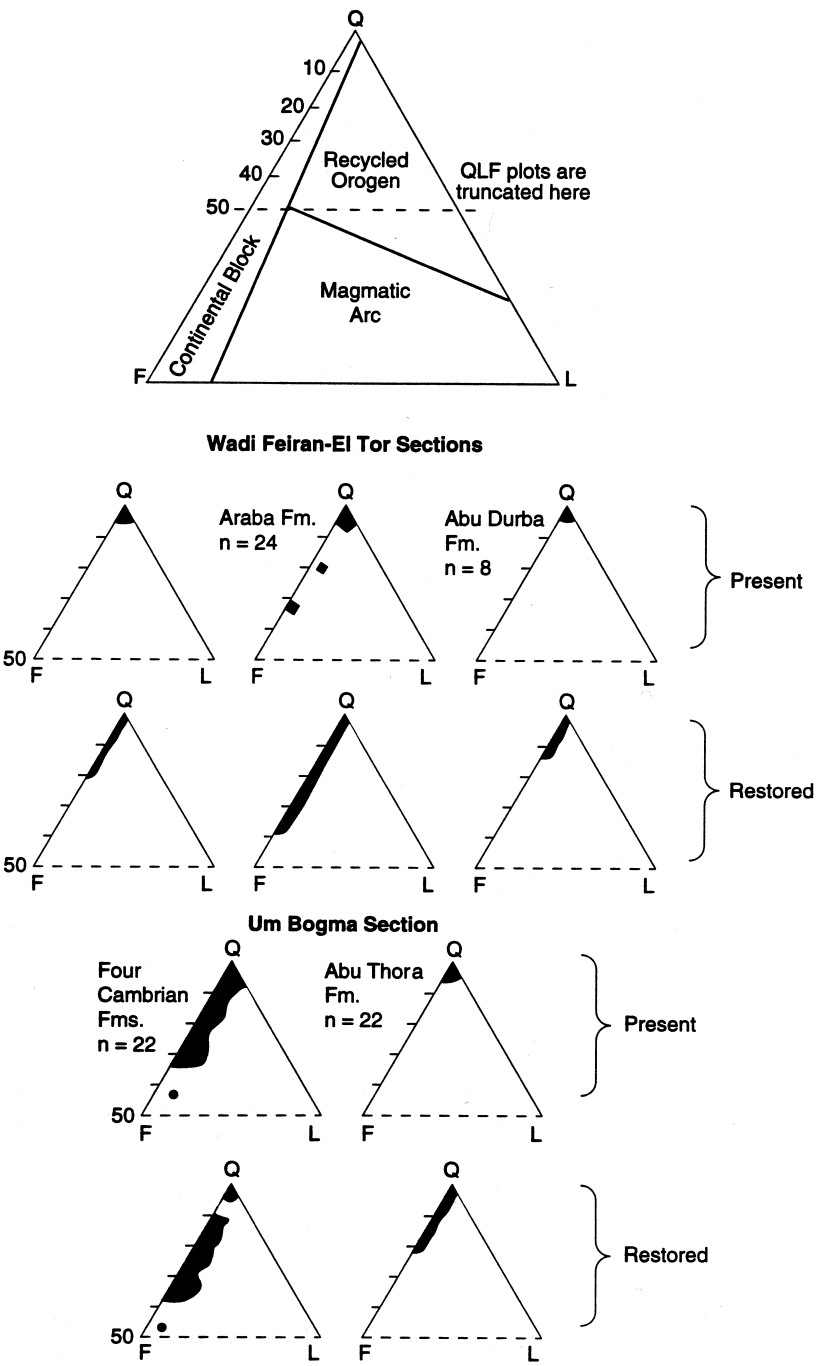

Fig. 5. Present and restored modal composition of sandstones. See text for restoration procedure. Provenance fields from Dickinson et al. (1983).

ments, mica, and heavy minerals are minor components in the samples. Present modal compositions are shown in Fig. 5. Point count data are available from the authors. We found no covariance of mineral composition with depositional environment, in part owing to extensive diagenetic overprinting of the rocks.

Mean framework grain size of the sandstones in all formations is primarily fine- to medium-grained, but is locally coarse. Most samples are unimodal, but some have a bimodal size distribution of the fine and coarse modes. This kind of bimodality, common in early Paleozoic rocks (Blatt, 1992, p. 67), is the product of an eolian history of abrasion and transportation (Folk, 1968; Johansen, 1988). Bimodality of eolian origin can survive marine transgression (Johansen, 1988).

Cements in the sandstone, in order of decreasing abundance, are iron oxides (hematite, goethite, maghemite), kaolinite, quartz, calcite, illite, smectite, mixed-layer illite–smectite, halite, gypsum, and barite. Only iron oxide, kaolinite, and quartz are common, though none are abundant with the exception of quartz cement in three silcretes. In the latter, quartz cement makes up from 8 to 36% in thin mature silcrete beds in the Naqus, Abu-Durba and Abu-Thora formations.

Porosities of both older and younger sandstones range from 1% to 27% and average 19%. The Naqus Formation, one of the older formations, is the chief hydrocarbon reservoir in the Gulf of Suez (Ibrahim, 1996).

5. Framework grains

Quartz makes up 78 to 99% of the sandstones sampled. The complete spectrum of quartz types (Folk, 1980, p. 69) is present, but common quartz, typical of plutonic and some metamorphic rocks, is by far the most abundant. Many polycrystalline quartz grains and some highly undulose and fractured monocrystalline quartz grains are dissolved to various degrees.

Feldspar rarely exceeds 2% of the framework grains except in seventeen samples of the lower three stratigraphic units at UB and in two samples of the lower part of the Araba Formation. However, dissolution of feldspar by groundwater and replacement of feldspar by calcite has significantly modified original modal compositions. The pre-diagenetic framework composition was calculated by assuming that oversize pores, including those filled by kaolinite, were originally feldspar. Older sandstones lost an average of 7.5% feldspar and younger sandstones lost an average of 5.0% feldspar. Restored modal compositions of samples are shown in Fig. 5. Samples that became quartzarenites because of the dissolution or replacement of feldspar qualify for the designation of ‘diagenetic quartzarenite’ (McBride, 1987).

Feldspar is more abundant in finer-grained samples. Electron microprobe analyses of detrital feldspar grains average $Or_{93}Ab_{6.6}An_{0.2}$, which suggests derivation of the grains from plutonic and/or metamorphic rocks (cf. Travena and Nash, 1981). The Na_2O content is between 0.2 and 1.2 wt%, which indicates that there has been no albitization.

Rock fragments and mica average less than 1% of framework grains. In decreasing abundance they are metamorphic (schist), sedimentary (chert, shale rip-up clasts, and hematitic sandstone), volcanic (silicified and devitrified rhyolitic rocks), and plutonic (granite).

6. Matrix

Detrital clay is essentially absent in the samples except as rare claystone rip-up clasts and, locally, thin clay coatings (cutans) a few micrometers thick of kaolinite and lesser illite occur on detrital framework grains. The clay is pigmented by iron oxides, has particles oriented parallel with detrital grain surfaces or around the margin of pores, and in places forms meniscus-shaped pore bridges. These are characteristics of unfiltered clay, clay particles introduced in suspension when muddy water percolates into dry sand in non-marine environments (c.f. Matlack et al., 1989; Abdel-Wahab and Turner, 1991).

7. Porosity

Thin section porosity was divided into three categories: (1) intergranular pores; (2) oversized pores (pores larger than normal intergranular pores and comparable to the size of framework grains); and (3) intragranular dissolution pores. Of the 18% average pore space in thin-section, 69% is intergranular pores, 26% is oversized pores, and 5% is intragranular pores. In this study the term ‘secondary porosity’ refers to the total of intragranular pores plus oversized pores, whereas intergranular porosity refers to all porosity between grains, whether it is primary or

has resulted from the dissolution of pore-filling cement. Essentially all intergranular pores are thought to be primary in these sandstones.

Of the total present porosity in all samples, primary porosity averages 69% (13% absolute porosity) and secondary porosity averages 31% (6% absolute porosity). Most of the secondary porosity resulted from the partial to complete dissolution of detrital feldspar grains based on the remnants found within secondary pores. However, dissolution of calcite cement in a few samples contributed to the development of secondary porosity. A more detailed treatment of porosity and permeability of the sandstones is presented in McBride et al. (1996).

8. Cement and other authigenic minerals

Authigenic minerals are discussed below in their paragenetic sequence (Fig. 4) as determined by textural relations in thin sections and SEM. The generation of thin clay grain coats from mechanically unfiltered clay in fluvial environments preceded the formation of authigenic phases in a few samples.

8.1. Iron oxides

Hematite, with some co-existing goethite and minor maghemite, is the most abundant cement in the sandstones. It is highly variable in abundance, ranging from a trace to 40%. It averages 7% in 68% of the samples containing it (Table 2). Iron oxide occurs as evenly distributed grain coats, localized patches of cement, and locally as extensive pore fill in sufficient abundance to warrant the term ferricrete. The term ‘ferricrete’, as defined by Ollier and Galloway (1990), is assigned to material cemented by Fe-oxides. If we restrict the term ferricrete here to sandstones with more than 10% iron oxide, all formations except the Nasib Formation have them. Ferricretes can form either by pedogenic processes or by the precipitation of iron oxides from laterally flowing surface or groundwater. The textural features of the Paleozoic Sinai sandstones are those of groundwater ferricretes (Milnes et al., 1987; Wright et al., 1992; Abdallah et al., 1993), which form as the products of mobilization and segregation of iron during fluctuating water tables (Milnes et al., 1987). During a eustatic rise of the water table, groundwater levels rise and cause iron to be reduced into the mobile ferrous state. Iron segregates and, on lowering of the water table and oxidation, is fixed as ferric iron forming cement and nodules of hematite and goethite. The ferricretes in the sandstones we studied are about 1 m thick, extend laterally over hundreds of meters, and are parallel with the bedding. Thus, they formed prior to folding of the Carboniferous strata. They range in color from dark brown (7.5YR 3/2) to nearly black (N4). Paleomagnetic data from two non-ferricrete older sandstones yield pole positions that best fit Middle Cambrian time. Either the data are spurious or the Cambrian age advocated by some authors (noted earlier) for the older rocks is correct. Iron oxides occur in the Sinai ferricretes as spherical, tubular, or irregular concretions 5–10 cm in diameter and as crusts up to 5 cm thick along bedding planes and fractures. These forms are similar to forms described in other rocks by Abdallah et al. (1993). Tubular concretions 50 cm long have an E–W orientation that reflects the flow of groundwater toward the Gulf of Suez (cf. McBride et al., 1994).

Hematite and goethite occur as pore-filling and pore-lining textures (Figs. 6–9). Hematite occurs as microcrystals in several forms. Rosettes in which the crystals are blade-like and range from 1 to 3 μm in diameter and from 0.2 to 1 μm in width are common. They occur as interstitial pore-filling, pore-lining, and as drusy coatings, locally with botryoidal texture, on the surface of both detrital quartz grains and quartz overgrowths. Irregular aggregates of hematite crystals partly fill pore spaces and form coatings on quartz overgrowths. Samples with larger and more dense crystal clusters have the darkest red color (cf. Walker et al., 1981).

Table 2
Abundance of authigenic minerals

Mineral	% Samples with it	Range (%)	Mean (%)
Iron oxide	68	0–40	6.9
Quartz	91	0–8	2.2
Calcite	37	0–23	4.9
Kaolinite	70	0–20	6.1

Mean is only of samples containing the mineral. Quartz data exclude mature silcretes. Kaolinite includes dickite and cryptic porosity.

Fig. 6. Scanning electron micrograph of acicular goethite crystals. Locality AD.

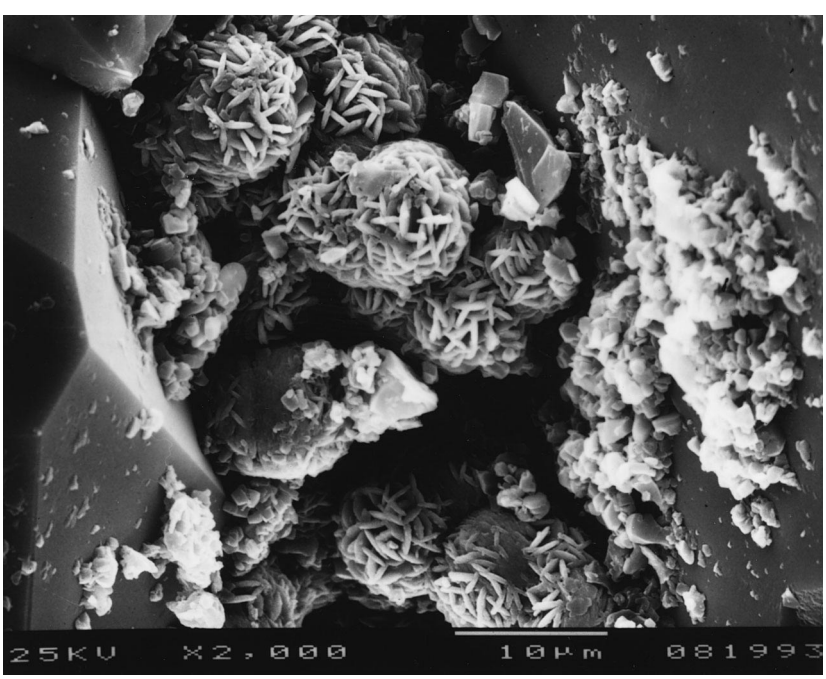

Fig. 7. Scanning electron micrograph of hematite rosettes showing the nature of individual crystals. Locality UB.

Fig. 8. Scanning electron micrograph of ball-like hematite crystals concentrated in a pore. Locality AD.

Fig. 9. Close-up view of the ball-like aggregates of hematite crystals in Fig. 8.

Goethite has an acicular habit and forms clusters of needle- or blade-like crystals 2–5 μm long and about 0.5 μm broad (Fig. 6). These acicular crystals most commonly occur together with small platelets of hematite 2–7 μm in diameter. Hematite forms rosettes (Fig. 7) and ball-like crystal clusters (Figs. 8 and 9).

Evidence of diagenetic origin for the iron oxide in these sandstones includes the following (cf. Walker, 1967): (1) iron oxide coatings on quartz and feldspar grains are absent at places of contact between grains; (2) iron-oxides coat authigenic minerals; (3) the delicate euhedral crystals of hematite and goethite as seen by SEM; and (4) hematite halos around biotite. Some iron may have been derived from ferrous minerals within the sandstones, but most of the iron must have been imported in groundwater. Evidence of an intraformational source includes item (4) above, and the suspicion that hornblende, whose alteration also produces iron oxide, might originally have been present as an accessory mineral in these sandstones that are derived from igneous and metamorphic terrain. The presence of partially dissolved and replaced feldspars indicates that grain alteration has progressed to the point that minerals more stable than ferromagnesian silicates have been altered.

Petrographic and paleomagnetic data indicate that the older sandstones underwent multiple episodes of iron-oxide generation. Hematite form coats on both detrital quartz grains and authigenic overgrowths, and possibly authigenic kaolinite. As noted above, paleomagnetic data from two Naqus samples from this study yield pole positions that best fit the Middle Cambrian (Salem, 1995). An additional sample of the Naqus sandstone from the western margin of the Gulf of Suez yields ages of magnetization of Carboniferous (~200 Ma) and Middle Cretaceous (60 Ma) time.

Pedogenic ferricretes typically develop under humid, seasonal tropical-type climates (Nahon, 1986, 1991), whereas groundwater ferricretes form under less humid to arid settings (Wright et al., 1992).

8.2. Quartz

Quartz cement occurs in all sandstones, ranging from trace amounts to 6% (mean 3%; Figs. 10 and 11), except in three mature silcretes, where it ranges from 8 to 36%. We identify three thin (<4 m thick) beds as mature silcretes on the basis of greater quartz cement abundance (>8%) plus the unusual silica cement phases: syntaxial quartz that is zoned optically and under cathodoluminescence (Figs. 12 and 13), microcrystalline quartz, and opal (now cryptocrystalline quartz). However, scattered throughout the formations studied are sandstones whose detrital quartz grains have thin layers of silica cements (microcrystalline quartz and rinds of opal [now pores] beneath microcrystalline quartz) whose textures are compatible with a silcrete origin. These are considered incipient silcretes.

8.2.1. Normal quartz cement

Quartz cement in these samples forms ordinary quartz overgrowths that developed morphologically in the manner described by Waugh (1970) and Pittman (1972; Figs. 10 and 11). In the earliest stage of cementation authigenic quartz formed 'blob-like' masses 2 to 3 μm long that lack crystal faces. With enlargement, the blobs formed crystal faces. Most quartz grains are only partly covered by patchy smooth overgrowths 30 to 40 μm long. Scanned cathodoluminescence shows that overgrowths are either unzoned or are characterized by sector zoning. A few samples have euhedral crystals 10 to 30 μm long that formed as neomorphic crystals that do not have detrital nuclei.

The stratigraphic distribution of quartz cement is shown in Fig. 3. Except for the three mature silcretes, quartz cement is relatively uniform in abundance in the AD and N sections. There is no obvious textural or stratigraphic control on the distribution of normal quartz cement.

The $\delta^{18}O$ value for normal quartz cement and detrital quartz grains determined from the data shown in Fig. 14B is 30.5‰ (SMOW) and 12.7‰, respectively. If the 30.5‰ is a reliable average value for the oxygen composition of the cement, the data are compatible with cement precipitating at 43ºC from sea water, at 34ºC from meteoric water with a $\delta^{18}O$ of −2‰, and at 26ºC from meteoric water with a $\delta^{18}O$ of −4‰. We found no fluid inclusions to constrain the salinity of the cementing fluids. However, several lines of evidence indicate that quartz cementation in these sandstones took place in meteoric waters. Evidence includes: (1) normal quartz

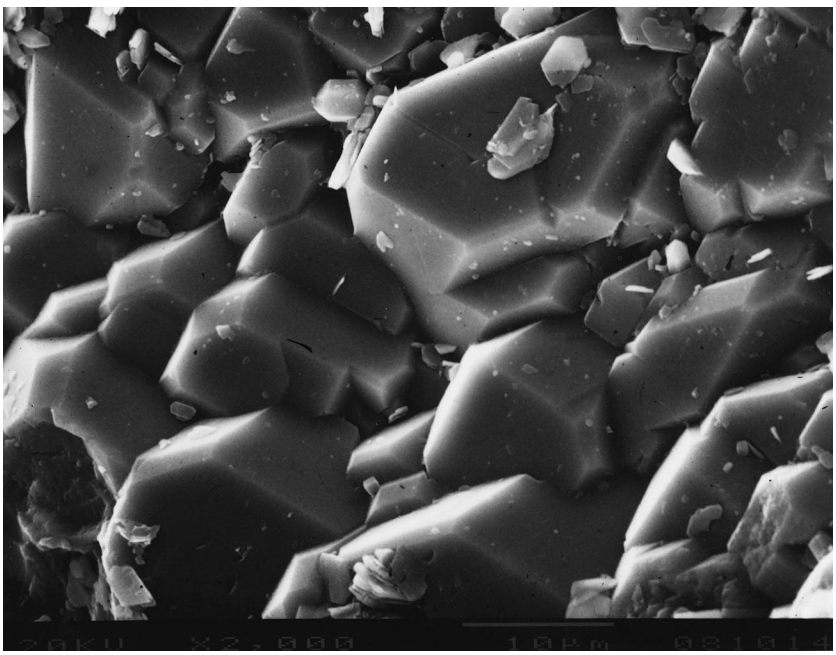

Fig. 10. Quartz cement forms ordinary quartz overgrowth subcrystals 3–5 μm long.

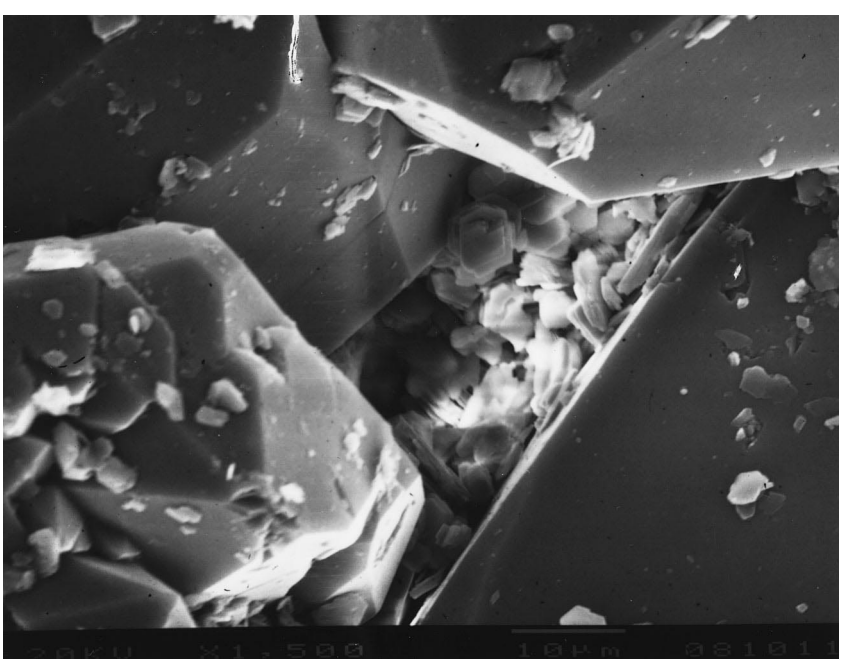

Fig. 11. Smooth, well-defined crystal faces (30–40 μm) in quartz overgrowths. Scale bar is 10 μm. Locality UB.

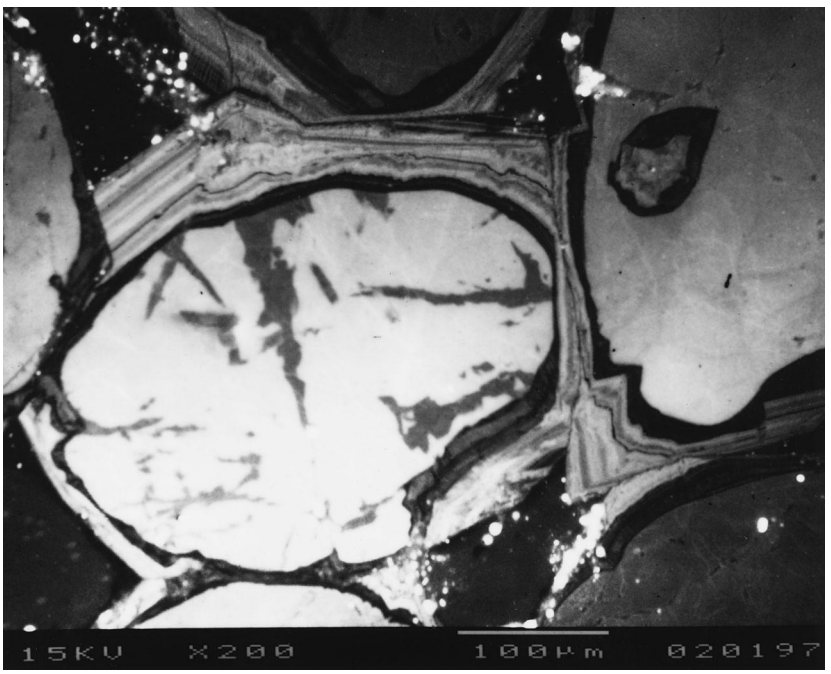

Fig. 12. Scanned CL image showing luminescing detrital quartz grains coated first by a faint- to non-luminescing overgrowth then by a brightly luminescing and stratigraphically zoned overgrowth. Locality N.

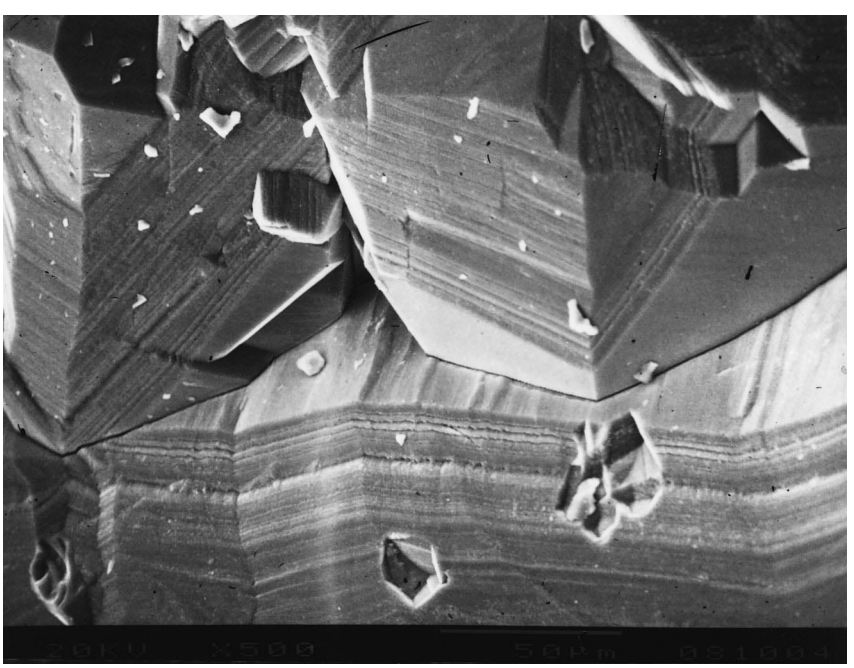

Fig. 13. Scanning electron micrograph showing microsteps reflecting successive zones (>40) in quartz overgrowth in silcrete. Scale bar is 50 μm. Locality N.

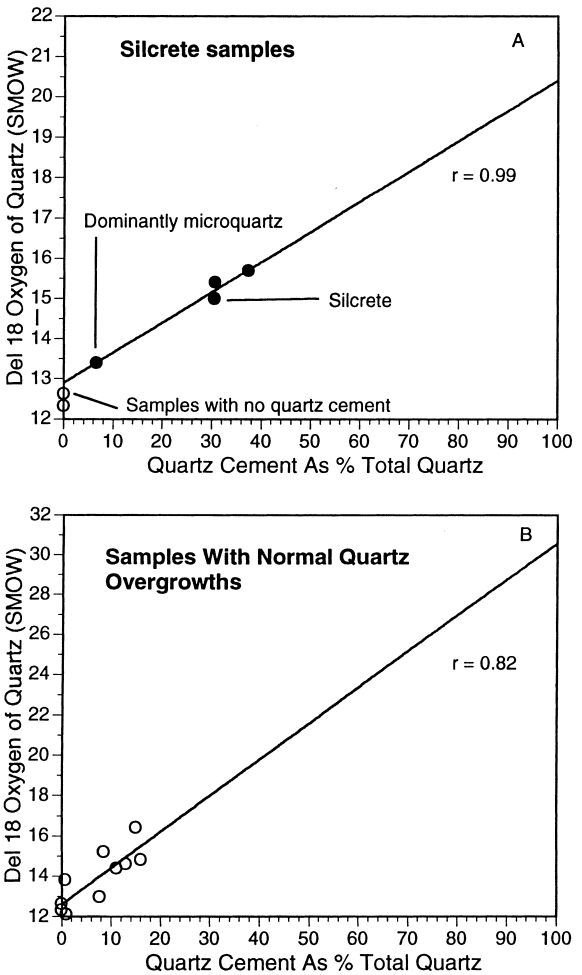

Fig. 14. Crossplot of $\delta^{18}O$ values and percent of quartz overgrowth/total quartz for silcrete (A) and normal quartz cement (B).

cement is overprinted by silcrete quartz of meteoric origin; (2) oxygen isotopic values for calcite and kaolinite cements, both younger than quartz cement, have meteoric signatures; (3) iron oxide of meteoric origin both preceded and overprinted normal quartz cement; and (4) the Carboniferous formations are truncated by an unconformity, which would permit meteoric water influx. The Sinai region migrated from approximately 35ºS during the Carboniferous to the Equator by Cretaceous time (Paleomap, 1992). If cementation was by meteoric water of −2‰ to −4‰ $\delta^{18}O$ and the average surface temperature was 20º to 25ºC at the latitudes indicated, temperatures of 26ºC to 34ºC could be found from the surface to a depth of only several hundred meters.

8.2.2. Quartz in mature silcretes

Mature silcretes occur in each of the following three sections: the uppermost cap of hard Naqus sandstone at N (4 m thick); the directly overlying black shales of the Abu-Durba Formation (2 m thick) at AD; and the uppermost bed of Abu-Thora sandstone (1 m thick) (Salem, 1995; Abdel-Wahab et al., 1998). The silcretes of this study have grain-supported fabrics, preserve original bedding, but lack illuviation features (clay cutans). They are cemented entirely by zoned syntaxial quartz (Fig. 13, Naqus) or by a combination of syntaxial quartz and microcrystalline quartz (Abu-Durba) or by both phases plus opal (Abu-Thora). These silica phases overprint a percent of two of normal quartz cement. Under cathodoluminescence, syntaxial quartz in the Naqus records multiple zones of strong versus weak luminescence (Fig. 12). Such zones reflect variations in trace elements or lattice defects (Matter and Ramseyer, 1985) in the authigenic quartz, which reflects variations in water composition during the time of precipitation (Murray, 1990).

The isotopic composition of quartz in the silcrete samples is +20.5‰ (Fig. 14A). This depleted $\delta^{18}O$ value for overgrowths is compatible with precipitation of quartz from meteoric water with a $\delta^{18}O$ value of −2‰ at 88ºC or with a value of −4‰ at 75ºC. These temperatures reflect either near-surface thermal waters or pore waters at burial depths of 1.8 to 2.3 km if the surface temperature and geothermal gradient were the same as assumed for the non-silcretes. We were unable to find fluid inclusions in overgrowths to constrain the salinity of the precipitating waters. Several features of the beds interpreted as silcretes differ from quartz cement that forms normally during burial, i.e. the complex stratigraphic zonation of megaquartz overgrowths in the Naqus silcrete, the presence of microcrystalline quartz and opal, the lack of correlation of abundance of quartz cement with depth, and the restriction of strongly cemented beds to such thin intervals. Thus, the evidence strongly favors the interpretation that cementation was by shallow thermal meteoric waters that were horizontally stratified. The Late Triassic–Early Jurassic basalt intrusions (Weissbrod, 1969)

may have provided the heat for this thermal event. Stratigraphic evidence indicates that the silcretes are pre-Cretaceous (Abdel-Wahab et al., in press).

The silcretes have some mineralogical features of pedogenic silcretes (e.g. Smale, 1973; Summerfield, 1983; Thiry and Millot, 1987), but textural aspects of groundwater silcretes. Evidence for cementation from horizontally stratified thermal waters also precludes a pedogenic origin. Following Millot (1960), Summerfield (1983), and Williams and Crerar (1985), we attribute megaquartz in silcrete to precipitation from groundwater low in silica and low in impurity ions in contrast with microquartz and opal, which precipitate from water enriched in dissolved silica and impurity ions.

8.2.3. Sources of silica

The only potential sources of silica for quartz cement within the sandstones are from dissolved and replaced feldspars and the dissolution of detrital quartz grains. Sutured detrital grain contacts are rare and stylolites are absent, indicating that pressure solution was unimportant. Although partially dissolved quartz grains (chiefly polycrystalline grains) are widespread, they are not abundant. Thus, the amount of silica released by dissolution of detrital quartz grains is insignificant.

Mass balance calculations (Salem, 1995) show that enough silica was released during the dissolution of feldpars to provide the amount of quartz cement in the lightly cemented sandstones. However, much of the Al and Si released during feldspar dissolution ended up in authigenic kaolinite, and, more importantly, the time of kaolinite generation was much later than the time of quartz cementation. Thus, Si for normal quartz cement was introduced in meteoric groundwater. Silica for silcrete generation also had to be imported. The consensus is that silica in silcretes in general was derived from weathering reactions of silicate minerals, including clays, and dissolution of quartz in bedrock and alluvium (Summerfield, 1983; Thiry and Millot, 1987).

Ibrahim (1996) suggested that some silica was derived from clay mineral diagenesis from clays in interbeds in the Naqus in the subsurface. Some of his samples are from deeper than 3 km, where heat needed to drive the smectite–illite transformation is available.

8.3. K-feldspar

Authigenic K-feldspar is present as a minor constituent (generally $<1\%$, maximum of 3%) in the older sandstones, where it tracks the abundance of detrital feldspars. Authigenic K-feldspar occurs in three modes: overgrowths, discrete crystals, and coarse crystals cementing quartz grains. The later two modes lack detrital cores and are wholly authigenic, but both are rare.

K-feldspar overgrowths tend to form almost complete rhombohedral crystal faces, but occur in optical discontinuity with detrital grains and are untwinned. Overgrowths that range in size from 1–3 μm start as small rhombohedral crystals in the manner described by Worden and Rushton (1992). Microprobe analyses of K-feldspar overgrowths show they are virtually pure end-member $KAlSi_3O_8$ with average K_2O values of 16.5%. Overgrowths are approximately synchronous with quartz.

Authigenic feldspar attached to the surface of detrital quartz grains occurs only in the lower part of the Araba Formation, whereas free-standing rhombic crystals occur in some samples of the Abu-Hamata Formation. Both these types of authigenic crystals formed without a detrital seed crystal and probably precipitated from water with a higher level of supersaturation than that which formed normal overgrowths (cf. Ali and Turner, 1982; Abdel-Wahab and Turner, 1991). A Rb/Sr isochron dating of two samples of authigenic feldspar crystals from the Araba Formation yields a value of 48.4 ± 1.6 Ma (Eocene). If this date is correct, the neomorphic K-feldspar formed during the time of maximum burial of the rocks.

The source of K^+ for authigenic feldspar must be from detrital K-feldspar in the older sandstones themselves and possibly from K-feldspar in the underlying basement. Authigenic K-feldspar occurs in the alteration profile directly below the Cambrian–Precambrian unconformity of the North American mid-continent (Duffin, 1989). This raises the possibility that meteoric water transferred some K^+ from feldspars in the Sinai basement rocks to overlying sandstones. Quartz and feldspar cements are intergrown in places, so both formed from meteoric water.

8.4. Calcite

Non-ferroan authigenic calcite (both pore-filling and grain-replacing) has a very patchy distribution. Sixty percent of the samples have no calcite cement and only 5% have more than 12%. Two thirds of the calcite cement fills primary or secondary pores and the rest replaces framework grains, mainly feldspars. Calcite has a dull luminescence and is present as either micrite to fine spar (grains of 0.5 to 20 μm) or as poikilotopic spar with individual crystals reaching several millimeters in diameter. Both types of calcite occur as scattered tabular concretions less than 2 m long, many of which are made up of pea-size microconcretions.

Calcite cement formed after quartz cement. Both forms of calcite fill intergranular primary pores and oversized pores (up to 13%). Oversized patches of calcite formed by the replacement of feldspar grains with no preserved ghosts or filled the pores formed where feldspars dissolved after burial. Many of the K-feldspars in the Um-Bogma area show various degrees of calcitization around the periphery of the grain, along cleavages or in the centers of the grains. Detrital micas have been also invaded by calcite along cleavages to produce splayed ends.

No consistent differences in Mg, Fe, Mn, or Sr exist between pore filling and replacement calcite, a conclusion made for other rocks by others (e.g. Fisher and Land, 1986; McBride, 1987). Both poikilotopic calcite and fine-grained calcite show end-member calcite composition: $CaCO_3$ averages 97.3–99.8 mole percent, although fine-grained calcite is generally characterized by a slight enrichment in magnesium (comprising up to 3 mole percent $MgCO_3$). Fe and Mn were not detected, and Sr was detected only in the micritic calcite.

Carbon and oxygen isotopes were analyzed for both types of calcite (Table 3; Fig. 15). Poikilotopic calcite in Carboniferous sandstones could not be isolated because it occurs with micritic calcite. Each authigenic phase has a relatively distinct isotopic signature. $\delta^{18}O$ values of micritic calcite reach +2.3‰ but average +0.4‰ (PDB), whereas $\delta^{18}O$ values of poikilotopic calcite are chiefly between −10 and −12‰ (PDB). Likewise, $\delta^{13}C$ values in poikilotopic calcite are depleted (average −3.3‰ PDB), but range from 0 to +5‰ in micritic calcite.

Table 3
Isotopic composition of calcite cement

Sample	Calcite type	$\delta^{13}C$ (‰) PDB	$\delta^{18}O$ (‰) PDB	$\delta^{18}O$ (‰) SMOW	$^{87}/^{86}SR$
22 NQ	P	−5.3	−9.82	20.73	0.7086
56 NQ	P	−3.76	−10.58	19.95	
61 NQ	P	−3.88	−12.04	18.44	
65 NQ	P	−0.19	−3.28	27.47	0.7108
73 NQ	M	3.15	2.23	33.15	
60 D	M	0.48	−0.64	30.2	
74 D	M	2.96	0.23	31.09	
82 D	M	2.53	0.85	31.73	
87 D	B	−0.22	−7.52	23.1	0.7088
91 D	M	2.38	−2.31	28.47	
95 D	M	0.92	−2.01	28.78	
107 D	M	2.32	−0.49	30.35	0.7094
113 D	B	0.32	−3.62	27.12	
7 Um	M	4.09	2.3	33.23	
17 Um	M	4.04	1.19	32.08	
27 Um	M	2.25	−0.56	30.28	
35 Um	M	2.6	0.53	31.4	
45 Um	M	4.17	−0.42	30.42	
56 Um	M	3.02	−1.44	29.37	
70 Um	M	3.04	1.08	31.97	
92 Um	M	3.57	0.91	31.79	
103 Um	M	2.77	0.5	31.37	
108 Um	M	3.67	1.75	32.66	
114 Um	M	0.44	−1.46	29.35	
125 Um	M	2.37	0.42	31.29	
130 Um	M	2.78	1	31.89	0.7084
142 Um	M	2.38	0.92	31.8	
145 Um	M	4.82	1.81	32.72	
154 Um	B	−1.07	−0.39	30.45	0.7091
163 Um	M	3.51	2.59	33.52	
Average	P	−3.28	−8.93	21.64	
Average	M	2.79	0.39	31.26	
Average	B	−0.32	−3.84	26.89	

P: poikilotopic; M: microcrystalline; B: both.

Samples with both types of calcite cements have compositions that fall between the end members.

Micritic calcite has $\delta^{18}O$ values commensurate with precipitation from sea water to evaporitic brines at surface temperatures. The heaviest micritic calcite precipitated from brine with a $\delta^{18}O$ of about +6‰ (SMOW) if the temperature was 34ºC (Fig. 16). Sea water and evaporite brines must have invaded the sandstones during highstands of sea level. The brines had been flushed by meteoric water by the time poikilotopic calcite precipitated. The depleted oxygen

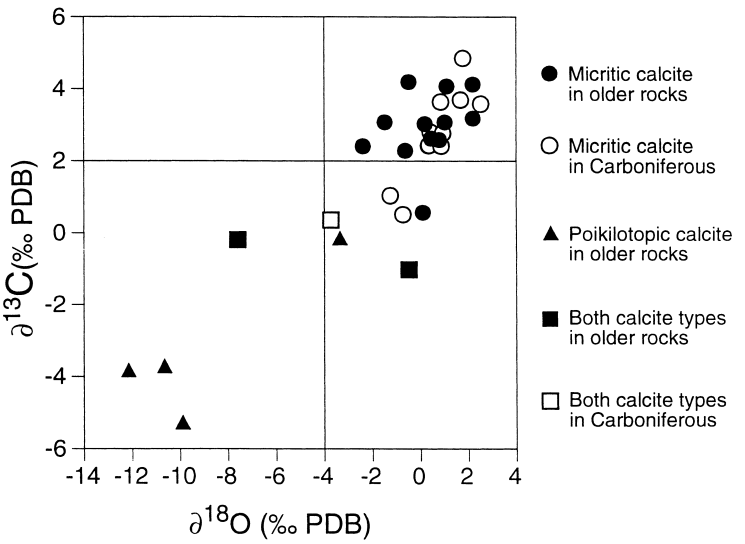

Fig. 15. Crossplot of $\delta^{13}C$ and $\delta^{18}O$ isotopic values for calcite cement.

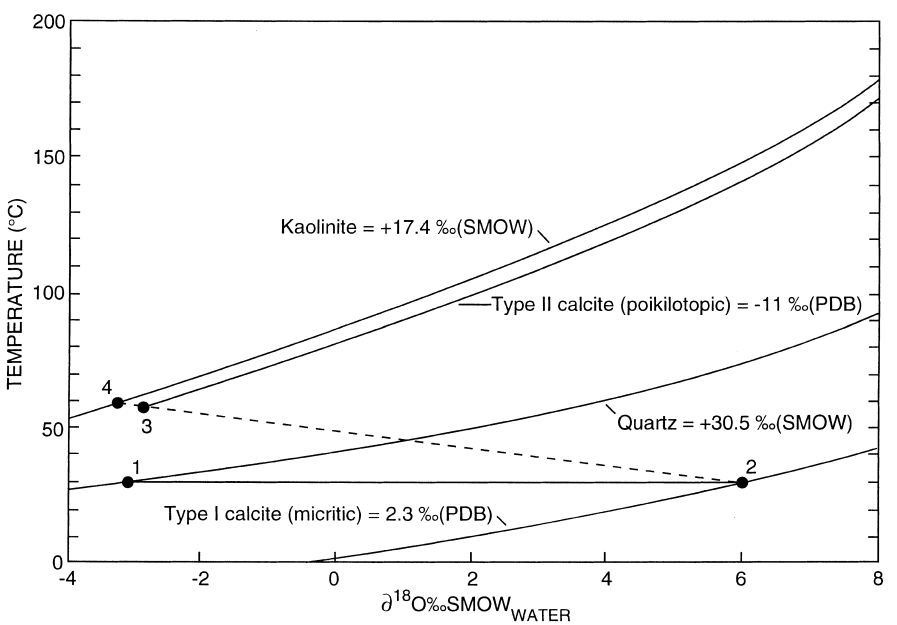

Fig. 16. Plot of oxygen isotopic data for quartz, calcite, and kaolinite showing possible relations to $\delta^{18}O_{water}$ and temperature. Probable evolution path of $\delta^{18}O$ of diagenetic water and conditions of cement precipitation (circled, numbered) are shown; dashed line indicates effect of meteoric flushing after precipitation of Type I calcite. Fractionation factors are from Clayton et al. (1972) for quartz, Friedman and O'Neil (1977) for calcite, and Land and Dutton (1978) for kaolinite.

isotopic values can best be attributed to precipitation from meteoric water rather than sea water (~0‰, SMOW) or diagenetically evolved water (~2‰), because the latter require temperatures of 75° to 108°C, temperatures higher than permitted for our burial data. Assuming that meteoric water had a $\delta^{18}O$ value of −2 to −4‰ (SMOW), then the temperature of precipitation of spar from older samples was from 47 to 74°C (Fig. 16). Taking average values for calcite (−11‰) and water (−3‰ SMOW), calcite formed

at 58ºC. If the surface temperature was 20ºC and water had an isotopic value of −3‰, spar cement formed at a depth of ~1.3 km. The inferred time of spar formation is close to the onset of rifting of the craton, when meteoric recharge in uplifted terrain would be possible.

Carbon isotopic values of micritic calcite indicate carbon was derived from both sea water (values near 0‰) and from a minor component of heavy carbon such as is formed during methanogenesis (Curtis et al., 1986). For poikilotopic calcite, the slightly depleted $\delta^{13}C$ values (mean −3.3‰) indicate that a small amount of carbon was derived from organic matter degradation and the rest was probably derived from marine carbonate.

$^{87/86}Sr$ ratios were determined for calcite in six samples to help constrain the cementation processes (Table 3). One sample of sparry calcite and one micritic sample have ratios ≥0.7094, indicating that cementation occurred in these samples from water that had reacted with radiogenic silicates, probably K-feldspar. The remaining two younger samples of micritic or mixed micritic–sparry calcite yield isotopic values typical of early Paleozoic or late Tertiary sea water according to the curve of Burke et al. (1982). Neither of these ages are feasible times of cementation or feasible ages of limestone that might have provided calcite for cement. These spurious values probably reflect admixture of non-radiogenic Sr and radiogenic Sr released during K-feldspar alteration. The remaining two older samples are dominated by sparry calcite of meteoric origin, for which the Sr ratio clock is inappropriate.

The source of marine carbon for micritic cement was the sea water and brines that invaded the sands during highstand events, but the source of marine carbon and also calcium in sparry poikilotopic calcite is not clear. Possible the marine sandstones in the formations studied originally contained enough shell material to supply these components.

8.5. Kaolinite

Authigenic clays present include kaolinite, illite and smectite; chlorite is reported from the Naqus in the subsurface (Ibrahim, 1996). Illite and smectite constitute trace amounts only in the lower sandstone series of the Um-Bogma sequence; they are not discussed further. Kaolinite averages 5.8% in older sandstones but only 0.2% in younger sandstones (Table 2). Values of kaolinite reported from point counts do not reflect the cryptic microporosity between clay platelets, which can reach 60% (Hurst and Nadeau, 1995). Kaolinite occurs as pore lining, pore filling (Figs. 17 and 18), replacement of feldspar, alteration product of muscovite, and grape-size concretions. Kaolinite commonly occurs in the form of face-to-face stacking of microporous pseudohexagonal plates (2–20 μm in diameter). Kaolinite also occurs as vermicular crystals, blocky crystals and orderly stacked crystals where the individual cleavage plates tend to be aligned along the *c*-axis direction. The kaolinite polymorph dickite was identified in some samples by XRD, but no attempt was made to quantify its abundance.

The euhedral morphology of the crystals indicates their authigenic origin. A few kaolinite particles are engulfed in quartz overgrowths and formed synchronously with quartz, but most kaolinite rests on quartz and postdates it.

Kaolinization of detrital K-feldspars is common and ranges from partial to complete replacement by kaolinite. Some detrital muscovite grains have been extensively replaced by kaolinite at their splayed ends and along cleavage planes (Fig. 18). Kaolinized muscovite displays all gradations between fresh grains with only expanded edges to masses of tightly packed kaolinite sheaves reflecting complete muscovite kaolinization.

The oxygen isotopic composition of kaolinite (including some dickite) ranges from 16.3 to 18.7‰ with an average of 17.4‰. This value is compatible with the precipitation of the kaolinite from meteoric water at a temperature of 63ºC and a $\delta^{18}O$ of −2‰ (SMOW) or at 52ºC with a $\delta^{18}O$ of −4‰ (Fig. 16). The burial curve for the rocks shows that these temperatures were not reached until Cretaceous or early Tertiary times. Considering the long time that the sandstones were buried less than 700 m, the question arises why most kaolinite did not form until late diagenesis and deeper burial. However, significant relief in the area did not form until rifting generated the Red Sea and marginal uplifts beginning in the Miocene (Purser et al., 1993). This newly generated relief permitted a deeper invasion of meteoric water and promoted the generation of kaolinite.

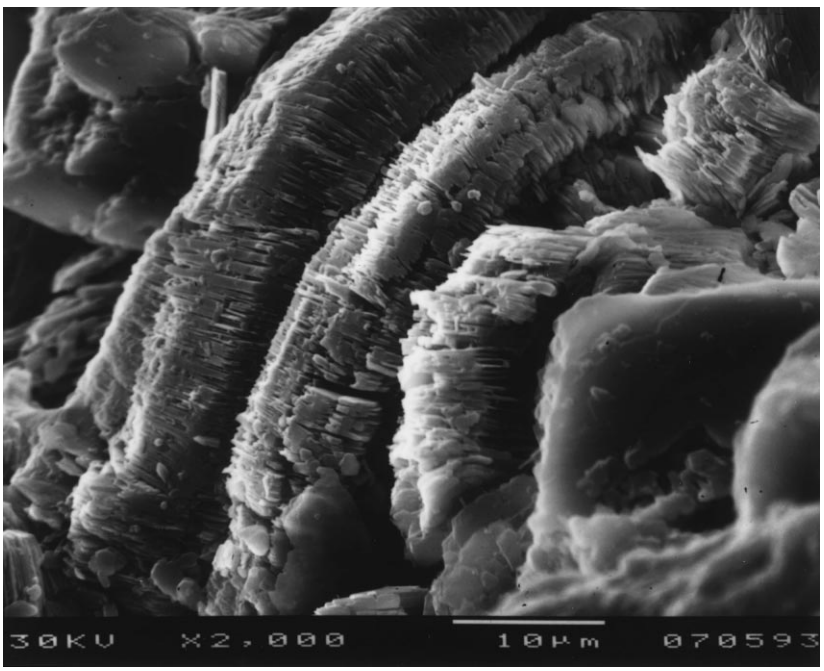

Fig. 17. Electron micrograph showing a vermicular kaolinite cluster filling the pore space. Locality AD.

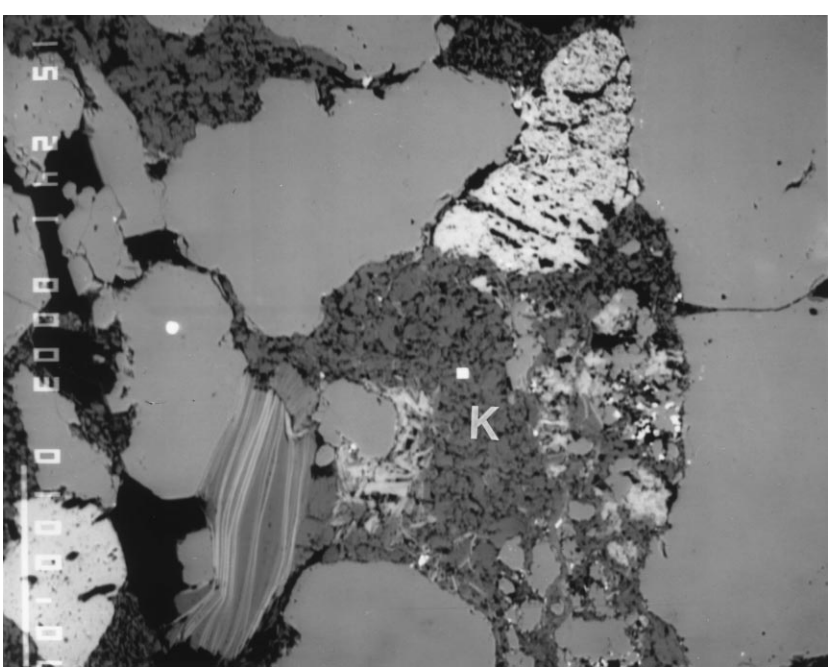

Fig. 18. Backscattered electron micrograph of sandstone with patches of microporous blocky vermicular kaolinite crystals (*K*) and a partially kaolinized muscovite (banded grain). Unaltered muscovite sheets (light tone) have been separated by kaolinized sheets (dark tone). Scale bar is 100 μm. Locality UB.

SEM images show that a small amount of kaolinite formed simultaneously with quartz cement.

The most likely source of Al and Si for kaolinite is from dissolved detrital K-feldspar. This transformation has been treated quantitatively by several authors (Bjørlykke, 1983; Curtis, 1983; Hayes and Boles, 1992). If feldspar dissolution proceeds by the following formula (Hayes and Boles, 1992):

$$2KAlSi_3O_8 + 2H^+ + H_2O \rightarrow Al_2Si_2O_5(OH)_4 + 2K^+ + 4SiO_2 \quad (1)$$

then each unit volume of K-feldspar yields 0.5 volumes of kaolinite. The 7.5% K-feldspar lost from older sandstones and 5% lost from younger sandstones could have yielded 3.8% and 2.5% kaolinite, respectively. Assuming that kaolinite in our samples has 50% cryptic porosity, then the actual volume of kaolinite in our samples is 2.9% in older rocks and 0.1% in younger rocks. Thus, there is slightly less kaolinite present in older sandstones than predicted from the amount of K-feldspar dissolved, but much less kaolinite than predicted in younger sandstones. Large amounts of aluminum and silica were exported from younger sandstones.

Kaolinite in the Naqus in the subsurface was attributed by Ibrahim (1996) to both feldspar alteration and direct precipitation from pore fluids.

8.6. Barite, halite, and gypsum

Barite occurs in one sample at the base of Abu-Durba Formation as clusters of spherical concretions 2–8 cm in diameter. Barite precipitated as pore-filling cement with a radial growth habit. It replaced or grew around kaolinite.

Halite cement occurs in both the Araba and Naqus formations at N and AD, but in only four samples. It occurs as a pore filling cement, but is presently undergoing dissolution, so that its original extent is unknown. The only other reported occurrences of halite cement in sandstones in outcrop are also from rocks marginal to the Gulf of Suez (Abdel-Wahab and McBride, 1990, 1991).

Gypsum forms scattered patches of cement in six older samples. Most patches are at the millimeter scale, but locally gypsum forms clusters of spherical concretions at the centimeter scale. Gypsum forms sparry and poikilotopic crystals of a prismatic or platy shape that fill primary and secondary pores.

Textural relations indicate that these three minor cements are late events, but barite preceded the evaporite minerals. There are several possible sources for the sulfate and chloride salts in these rocks: (1) recycled from uplifted Miocene evaporites, (2) sea water transgression during the Carboniferous or younger time, and (3) sea spray and air-borne salts. Starinsky et al. (1983) conclude that the only possible major source of salts in present-day groundwater in western Sinai is air-borne particles that are derived from carbonate beach sands and sabkha sediments along the coast of the Sinai Peninsula. The dissolved minerals are halite, gypsum, anhydrite, barite, calcite and aragonite. About 10% of the salts in water are derived directly from sea spray, while 90% originate from air-borne salts. Abdel-Wahab and McBride (1991) favored the hypothesis that the evaporite cements in the sandstones described here were recycled from Miocene rocks, but we are non-committal. Ibrahim (1996) found both barite and anhydrite in the Naqus in the subsurface and attributed them to derivation from unspecified overlying evaporites.

9. Porosity evolution

We assume that the initial porosity of these clean, well-sorted sandstones was 45% (Pryor, 1973; Atkins and McBride, 1992). This porosity was reduced by compaction and cementation. A previous study (McBride et al., 1996) found that the average amount of porosity loss due to compaction was approximately 19% (range 16% to 23%). That is, the intergranular volume was reduced to an average of 26% by compaction alone.

The degree of compaction shown by the Sinai Paleozoic sandstones is common for quartzose sandstones that do not undergo significant shallow cementation and which compact chiefly by grain rearrangement (Graton and Fraser, 1935; Füchtbauer, 1967).

The time of generation of secondary dissolution porosity is not well constrained. We cannot distinguish secondary pores formed during outcrop weathering from those formed during burial. Some dissolution of sparry calcite cement occurred. Some

kaolinite fills secondary pores, but this is likely the result of simultaneous dissolution of feldspar and precipitation of kaolinite. Given the long time that these permeable rocks were buried less than 1.5 km, there was ample opportunity for dissolution to occur.

10. Bleaching

There are several pieces of evidence that indicate that the white and tan sandstones were once 'red beds' that have been bleached: (1) red/non-red color boundaries cut across bedding, indicating that at least one color is secondary; and (2) in non-red sandstones, films of iron oxide are present inside detrital feldspar, rock fragments, and intraclasts, but are absent on the surfaces of grains. This distribution of iron oxide reflects the reduction and removal of ferric iron from grain surfaces easily accessible to reducing fluids, but the preservation or iron oxide in hidden sites within grains. Shales interbedded with non-red sandstones tend to retain sufficient iron oxide to be pale red or brown.

There was very little organic matter in the sandstones that could have served as a food source for reducing anaerobic bacteria, and meteoric groundwater is not normally capable of reducing ferric iron in goethite and hematite (cf. Freeze and Cherry, 1979, p. 247). The most likely reductant is H_2S (cf. Moulton, 1926; Keller, 1929; Machel and Burton, 1991) derived from the thermochemical maturation of organic matter in Mesozoic and Cenozoic shales and carbonates. Although these rocks are younger than the sandstones studied, they are more deeply buried than the sandstones within the margins of the Gulf of Suez rift. Hydrocarbons are being produced at present from several stratigraphic levels (Mahmoud Kholief, pers. commun., 1990). If H_2S was the reductant, the absence of pyrite or pyrrhotite in bleached beds raises the question of the fate of sulfur.

11. Discussion

In spite of their age (>285 Ma), quartzose and feldspathic Lower Carboniferous sandstones deposited on the Arabian shield in the western Sinai remain friable and porous except for strongly cemented ferricretes and silcretes. If the older sandstones are not Carboniferous as inferred herein, but are Cambrian as indicated by paleomagnetic data, then the time span of preserved porosity is extended to nearly 500 Ma. The most significant diagenetic changes were: (1) cementation by iron oxide that averages 7% but reaches 40% in groundwater ferricretes; (2) loss of 19% porosity by compaction; (3) generation of diagenetic quartzarenites by the loss of 7% detrital feldspar by kaolinization and dissolution; and 4) development of three thin mature silcretes apparently by thermal groundwaters. These fluvial and shallow-marine sandstones were not buried more than 1.5 km until Late Cretaceous and younger time, when the deepest rocks reached 2.5 km.

A review of the literature shows that the diagenetic and burial history of the Carboniferous Sinai sandstones contrasts markedly with most other Carboniferous sandstones. A summary of the characteristics of ten different stratigraphic units is given in Table 1. Most Carboniferous sandstones have been buried deeper, have maximum porosities <15%, are dominated by quartz and carbonate cements and lack iron oxide cements, and many have had no contact with meteoric water during diagenesis. Because of deposition of the Sinai sandstones on a stable craton, which resulted in shallow burial and episodic exposure or proximity to the surface, meteoric water dominated the pore system for 200 Ma and possibly longer: iron oxides formed during multiple diagenetic stages (and yield Carboniferous and Late Cretaceous paleomagnetic signatures), and oxygen isotopic data for authigenic quartz, sparry calcite, and kaolinite yield meteoric water signatures. Of the various authigenic phases present, only micritic calcite and evaporite minerals are incompatible with deposition from meteoric water. Meteoric water influx could have taken place during deposition of the non-marine sands, at the end of the Carboniferous when a regional unconformity developed, and when positive elements developed during late Paleozoic folding (Abdallah et al., 1992) and during the extensional tectonics that generated the Gulf of Suez beginning in the Miocene (Purser et al., 1993).

Sinai sandstones have high porosity (maximum of 25%, mean of 19%) because there were no major sources of Si, Ca, and HCO_3^{2-} in the pore waters

to generate much quartz or calcite cement. In addition, 6% secondary porosity was developed by the dissolution of feldspar and possibly some calcite. However, as shown by the Carboniferous Spiro Sandstone in the Arkoma basin, anomalously high porosity can be retained in deeply buried sandstones where there are protective coats of chlorite on detrital quartz grains (Spotl et al., 1996; Table 1).

Normal quartz overgrowths are minor (2.2%) and did not retard compaction. All the quartz cement probably formed within 500 m of the surface, where silica for quartz cement was introduced in meteoric groundwater. Oxygen isotopes of quartz cement in the three thin silcretes indicate that these sandstones were cemented by thermal waters. The heat source for the hot waters was probably basalt sills and dikes of Late Triassic–Early Jurassic age. The Tensleep Sandstone from the northern Rocky Mountains, USA, like Sinai sandstones, possibly was invaded by meteoric water for nearly 200 Ma (James, 1992; Table 1). Ultimately, however, the Tensleep was buried deeper than the Sinai sandstones, and average porosity is only 9% owing to strong cementation by quartz, anhydrite, and dolomite.

The presence of gypsum-cemented sandstones in outcrop is not unusual, but halite-cemented sandstones certainly are. The source of halite and gypsum cements in the Sinai sandstones are uncertain: recycled from topographically higher younger rocks or from aerosols from surf spray?

Acknowledgements

McBride's participation was supported by the Egyptian Cultural Education Bureau and J. Nalle Gregory Chair in Sedimentary Geology at the University of Texas at Austin. Leon Long furnished the radiometric age of feldspar; Larry Mack provided the Sr isotope values; Lynton Land provided oxygen isotopic values for quartz and kaolinite; Rachel Eustice provided isotopic values for calcite; Kitty Milliken assisted with microprobe work; Wulf Gose provided paleomagnetic data. The manuscript benefited from reviews by Tim Diggs, Andrew Hurst, and an anonymous referee.

References

Abdallah, A.M., Darwish, M., El Aref, M., Helba, A.A., 1992. Lithostratigraphy of the Pre-Cenomanian clastics of north Wadi Qena, Eastern Desert, Egypt. Proc. First Int. Conf. Geology of the Arab World 1, pp. 255–282.

Abdallah, A.M., Darwish, M., El-Araby, A., Gaupp, R., 1993. Diagenesis related to unconformities in Late Carboniferous/Permo–Triassic sediments of Northern Galala, Gulf of Suez, Egypt. In: Thorweihe, U., Schandelmeier, H. (Eds.), Geoscientific Research in Northeast Africa. Balkema, Rotterdam, pp. 345–349.

Abdel-Wahab, A.A., 1990. Fabric and compaction analysis of Araba and Naqus quartzarenites (Cambrian), Gebel Araba–Qabeliat Southwest Sinai, Egypt. Delta J. Sci. 14, 666–707.

Abdel-Wahab, A.A., McBride, F.F., 1990. Diagenesis of diagenetic quartzarenites, Gebel El-Zeit area, Gulf of Suez, Egypt (Abs.) Am. Assoc. Petrol. Geol. Bull. 74, 594.

Abdel-Wahab, A.A., McBride, E.F., 1991. Diagenetic control of reservoir quality of Araba and Naqus diagenetic quartzarenites (Cambrian), Gebel Araba–Qabeliat, Southwest Sinai, Egypt. Delta J. Sci. 15, 160–203.

Abdel-Wahab, A.A., Turner, P., 1991. Diagenesis of the Nubia Formation, Central Eastern Desert, Egypt. J. Afr. Earth Sci. 13, 343–358.

Abdel-Wahab, A.A., Allam, A., Kholief, M., Salem, A., 1987. Provenance of Gebel El-Zeit sandstones, Gulf of Suez, Egypt. 26th Annu. Meet., Geol. Soc. Egypt, Cairo, Abstr., p. 30.

Abdel-Wahab, A.A., Allam, A., Kholief, M., Salem, A., 1992. Sedimentological and paleoenvironmental studies on the clastic sequence of Gebel El-Zeit area, Gulf of Suez, Egypt. J. Afr. Earth Sci. 14, 121–129.

Abdel-Wahab, A.A., Salem, A.M.K., McBride, E.F., 1998. Quartz cement of shallow origin in silcrete and non-silcrete sandstones, Lower Carboniferous, western Sinai, Egypt. J. Afr. Earth Sci. (in press).

Ali, A.D., Turner, P., 1982. Authigenic K-feldspar in the Bromsgrove sandstone Formation (Triassic) of Central England. J. Sediment. Petrol. 52, 187–197.

Allam, A., 1989. The Paleozoic sandstones in Wadi Feiran–El Tor area, Sinai, Egypt. J. Afr. Earth Sci. 9, 49–57.

Atkins, J.E., McBride, E.F., 1992. Porosity and packing of Holocene river, dune, and beach sands. Am. Assoc. Pet. Geol. Bull. 76, 339–355.

Bjørlykke, K., 1983. Diagenetic reactions in sandstones. In: Parker, A., Sellwood, B.W. (Eds.), Sediment Diagenesis. Reidel, Dordrecht, pp. 169–213.

Blatt, H., 1992. Sedimentary Petrology. Freeman, New York, 2nd ed., 514 pp.

Burke, W.H., Denison, R.E., Hetherington, E.A., Koepnick, R.B., Nelson, H.F., Otto, J.B., 1982. Variation of seawater $^{87}Sr/^{86}Sr$ throughout Phanerozoic time. Geology 10, 516–519.

Clayton, R.N., O'Neil, J.R., Mayeda, T.K., 1972. Oxygen isotope exchange between quartz and water. J. Geophys. Res. 77, 3057–3067.

Curtis, C.D., 1983. Link between aluminum mobility and de-

struction of secondary porosity. Am. Assoc. Petrol. Geol. Bull. 67, 380–393.

Curtis, C.D., Coleman, M.L., Love, L.G., 1986. Pore water evolution during sediment burial from isotopic and mineral chemistry of calcite, dolomite and siderite concretions. Geochim. Cosmochim. Acta 50, 2321–2334.

Deng, X., Sun, Y., Lei, X., Lu, Q., 1996. Illite/smectite diagenesis in the NanXiang, Yitong, and north China Permian–Carboniferous Basin: application to petroleum exploration in China. Am. Assoc. Pet. Geol. Bull. 80, 157–173.

Dickinson, W.R., Beard, L.S., Brackenridge, G.P., Erjavec, J.L., Ferguson, R.C., Inman, K.F., Knepp, R.A., Lindberg, R.A., Ryberg, P.T., 1983. Provenance of North American Phanerozoic sandstones in relation to tectonic setting. Geol. Soc., Am. Bull. 94, 222–235.

Duffin, M.E., 1989. Nature and origin of authigenic K-feldspar in Precambrian basement rocks of the North American midcontinent. Geology 17, 765–768.

Dutton, S., Land, L.S., 1985. Meteoric burial diagenesis of Pennsylvanian arkosic sandstones, southwestern Anadarko Basin, Texas. Am. Assoc. Pet. Geol. Bull. 69, 22–38.

Dutton, S.P., Clift, S.J., Folk, R.L., Hamlin, H.S., Marin, B.A., 1993. Porosity preservation by early siderite cementation in Sonora Canyon sandstones, Val Verde Basin southwest Texas. Am. Assoc. Pet. Geol. Annu. Meet., New Orleans, p. 95.

Eames, L.E., 1984. Palynologic definition of Paleozoic unconformity bounded sequences, Gulf of Suez region, Egypt, 7th Petroleum Exploration and Production Conf. (EGPC), Cairo, Vol. 1, pp. 117–125.

Eyal, M., Bartov, Y., Shimron, A.E., Bentor, Y.K., 1980. The Geologic map of Sinai, scale 1 : 500,000. Geological Society of Israel, Annual Meeting, Ophira programme, Abstr., p. 9.

Fisher, R.S., Land, L.S., 1986. Diagenetic history of Eocene Wilcox sandstones, South-Central Texas. Geochim. Cosmochim. Acta 50, 551–561.

Folk, R.L., 1968. Bimodal supermature sandstones: product of the desert floor. 23rd Int. Geol. Congr. Proc., Section 8, pp. 9–32.

Folk, R.L., 1980. Petrology of Sedimentary Rocks. Hemphill, Austin, Texas, 182 pp.

Freeze, R.A., Cherry, J.A., 1979, Groundwater. Prentice Hall, Englewood Cliffs, N.J., 604 pp.

Friedman, I., O'Neil, J.R., 1977. Compilation of stable isotope fractionation factors of geochemical interest. In: Fleischer, M. (Ed.), Data of Geochemistry, 6th ed., U.S. Geol. Surv. Prof. Pap. 440-KK, 12 pp.

Füchtbauer, H., 1974. Zur Diagenese fluviatiler Sandsteine. Geol. Rundsch. 63, 904–925.

Füchtbauer, H., 1967. Influence of different types of diagenesis on sandstone porosity. 7th World Petroleum Congr. Proc. 2, 353–369.

Graton, L.C., Fraser, H.J., 1935. Systematic packing of spheres with particular relation to porosity and permeability. J. Geol. 66, 391–416.

Hamlin, H.S., Dutton, S.P., Seggie, R.J., Tyler, N., 1996. Depositional controls on reservoir properties in a braid-delta sandstone, Tirrawarra oil field, south-Australia. Am. Assoc. Pet. Geol. Bull. 80, 139–156.

Hansely, P., 1996. Patterns of diagenesis in lower and middle Pennsylvanian sandstones of Illinois Basin, Illinois, Indiana, and Kentucky. U.S. Surv. Bull. 2094, E1–31.

Hayes, M.J., Boles, J.R., 1992. Volumetric relations between dissolved plagioclase and kaolinite in sandstones: implications for aluminum mass transfer in the San Joachim basin, California. In: Houseknecht, D.W., Pittman, E.D. (Eds.), Origin, Diagenesis, and Petrophysics of Clay Minerals in Sandstones. Soc. Econ. Paleontol. Mineral. Spec. Publ. 47, 111–124.

Hurst, A., Nadeau, P.A., 1995. Clay microporosity in reservoir sandstones: an application of quantitative electron microscopy in petrophysical evaluation. Am. Assoc. Pet. Geol. Bull. 79, 563–573.

Ibrahim, A.A.E., 1996. Petroleum Geology of the Cretaceous and Pre-Cretaceous Sediments in Some Oil Fields in the Gulf of Suez Area, A.R. Egypt. Unpubl. PhD dissertation, Cairo University, 211 p.

James, W.C., 1992. Sandstone diagenesis in mixed siliciclastic–carbonate sequences: Quadrant and Tensleep Formation (Pennsylvanian), northern Rocky Mountains. J. Sediment. Petrol 62, 810–824.

Johansen, S.J., 1988. Origins of upper Paleozoic quartzose sandstones, American southwest. Sediment. Geol. 56, 153–166.

Keller, W.D., 1929. Experimental work on red bed bleaching. Am. J. Sci. 5, 65–70.

Klitzsch, E., 1990. Paleozoic. In: Said, R. (Ed.), The Geology of Egypt. Balkema, Rotterdam, pp. 393–406.

Land, L.S., 1984. Frio sandstone diagenesis, Texas Gulf Coast. A regional isotopic study. In: McDonald, D.A., Surdam, R.C. (Eds.), Clastic Diagenesis. Am. Assoc. Petrol. Geol. Mem. 37, 47–62.

Land, L.S., Dutton, S.P., 1978. Cementation of a Pennsylvanian deltaic sandstone: isotopic data. J. Sediment. Petrol. 48, 1167–1176.

Lynch, F.L., 1994. The Effects of Depositional Environment and Formation Water Chemistry on the Diagenesis of Frio Formation (Oligocene) Sandstones and Shales, Aransas, Nueces, and San Patricio Counties, Texas. Unpubl. PhD dissertation, Univ. of Texas at Austin, Austin, 303 pp.

Machel, H.G., Burton, E.A., 1991. Causes and spatial distribution of anomalous magnetization in hydrocarbon seepage environments. Am. Assoc. Pet. Geol. Bull. 75, 1864–1876.

Mart, J., Sass, E., 1972. Geology and origin of the manganese ore of Um-Bogma, Sinai, Egypt. Econ. Geol. 67, 145–155.

Matlack, K.S., Houseknecht, D.W., Applin, K.R., 1989. Emplacement of clay into sand by infiltration. J. Sediment. Petrol 59, 77–87.

Matter, A., Ramseyer, K., 1985. Cathodoluminescence microscopy as a tool for provenance studies of sandstones. In: Zuffa, G.G. (Ed.), Provenance of Arenites. Reidel, Dordrecht, pp. 191–212.

McBride, E.F., 1987. Diagenesis of the Maxon sandstone (Early Cretaceous), Marathon region, Texas: a diagenetic quartzarenite. J. Sediment. Petrol 57, 98–107.

McBride, E.F., Kimberly, J.E., 1963. Sedimentology of the

Smithwick Shale (Pennsylvanian), eastern Llano region, Texas. Am. Assoc. Pet. Geol. Bull. 47, 1840–1854.

McBride, E.F., Picard, M.D., Folk, R.L., 1994. Oriented concretions, Ionian coast, Italy: evidence of groundwater flow direction. J. Sediment. Petrol. A64 (3), 335–540.

McBride, E.F., Abdel-Wahab, A.A., Salem, A.M.K., 1996. Influence of diagenesis on reservoir quality of Cambrian and Carboniferous sandstones, southwest Sinai, Egypt. J. Afr. Earth Sci. 22, 285–300.

Millot, G., 1960. Silica, silex, silicifications et croissance des cristaux. Bull. Serv. Carte Geol. Alsace Lorraine 13, 129–146.

Milnes, A.R., Bourman, R.P., Fitzpatrick, R.W., 1987. Petrology and mineralogy of laterites in southern and eastern Australia and southern Africa. Chem. Geol. 60, 237–250.

Moulton, G.F., 1926. Some features of redbed bleaching. Am. Assoc. Pet. Geol. Bull. 10, 304–311.

Murray, R.C., 1990. Diagenetic silica stratification in a paleosilcrete, North Texas. J. Sediment. Petrol. 60, 717–720.

Nahon, D.B., 1986. Evolution of iron crusts in tropical landscapes. In: Coleman, S.M., Dethier, D.P. (Eds.), Rates of Chemical Weathering. Acad. Press, San Diego, Calif., pp. 169–197.

Nahon, D.B., 1991. Introduction to the Petrology of Soils and Chemical Weathering. Wiley, New York, N.Y., 313 pp.

Ollier, C.D., Galloway, R.W., 1990. The laterite profile, ferricrete and unconformity. Catena 17, 97–109.

Paleomap, 1992. Paleogeographic Atlas. Department of Geology, University of Texas at Arlington, 30 pp.

Pittman, E.D., 1972. Diagenesis of quartz in sandstones as revealed by scanning electron microscopy. J. Sediment. Petrol. 42, 507–519.

Pryor, W.A., 1973. Permeability–porosity patterns and variations in some Holocene sand bodies. Am. Assoc. Pet. Geol. Bull. 57, 162–189.

Purser, B.H., Orszag-Sperber, F., Plaziat, J.C., Rioual, M., 1993. Plio–Quaternary tectonics and sedimentation in the SW Gulf of Suez and N. Red Sea. In: Thorweihe, U., Schandelmeier, H. (Eds.), Geoscientific Research in Northeast Africa. Balkema, Rotterdam, pp. 259–262.

Rezaee, M., Tingate, P., 1997. Origin of quartz cement in the Tirrawarra sandstone, southern Cooper Basin, south Australia. J. Sediment. Petrol. 67, 168–177.

Said, R., 1962. The Geology of Egypt. Elsevier, Amsterdam, 377 pp.

Salem, A.M., 1995. Diagenesis and Isotopic Study of the Paleozoic Clastic Sequence (Cambrian and Carboniferous), Southwest Sinai. Unpubl. Ph.D. thesis, Tanta University, 246 pp.

Shata, A., 1956. Structural development of the Sinai Peninsula, Egypt. Egypt. Desert Inst. Bull. 6, 117–157.

Smale, D., 1973. Silcretes and associated silica diagenesis in southern Africa and Australia. J. Sediment. Petrol. 43, 1077–1089.

Spotl, C., Houseknecht, D.W., Burns, S.J., 1996. Diagenesis for overmature gas reservoir: the Spiro sand of Arkoma Basin, USA. Mar. Pet. Geol. 13, 25–40.

Starinsky, A., Bielski, M., Ecker, A., Steinitz, G., 1983. Tracing the origin of salts in groundwater by Sr isotopic composition (the crystalline complex of the southern Sinai, Egypt). Isot. Geosci. 1, 257–267.

Summerfield, M.A., 1983. Petrography and diagenesis of silcrete from the Kalahari Basin and Cape Coastal Zone, Southern Africa. J. Sediment. Petrol. 53, 895–909.

Thiry, M., Millot, G., 1987. Mineralogical forms of silica and their sequence of formation in silcretes. J. Sediment. Petrol. 57, 343–352.

Travena, A.S., Nash, W.P., 1981. An electron microprobe study of detrital feldspar. J. Sediment. Petrol. 51, 137–150.

Walker, T.R., 1967. Formation of red beds in modern and ancient deserts. Geol. Soc. Am. Bull. 78, 353–368.

Walker, T.R., Larson, E.E., Hoblitt, R.P., 1981. Nature and origin of hematite in the Moenkopi Formation (Triassic), Colorado Plateau: a contribution to the origin of magnetism in red beds. J. Geophys. Res. 86, 317–333.

Waugh, B., 1970. Formation of quartz overgrowths in the Penrith sandstone (Lower Permian) of northwest England as revealed by scanning electron microscopy. Sedimentology 14, 309–320.

Weissbrod, T., 1969. The Paleozoic of Israel and adjacent countries, Part 2. The Paleozoic outcrops in southwestern Sinai and their correlation with those of southern Israel. Geol. Surv. Isr. Bull. 48, 32.

Weissbrod, T., 1980. The Paleozoic of Israel and Adjacent Countries (Lithostratigraphic Study). Ph.D. thesis, Hebrew Univ., Jerusalem, 276 pp. (non-vide) (in Hebrew with English abstract).

Williams, L.A., Crerar, D.A., 1985. Silica Diagenesis, II. General mechanisms. J. Sediment. Petrol. 55, 312–321.

Worden, R.H., Rushton, J.C., 1992. Diagenetic K-feldspar textures: a TEM study and model for diagenetic feldspar growth. J. Sediment. Pet. 62, 779–789.

Wright, V.P., Sloan, R.J., Garces, B.V., Garvie, L.A.J., 1992. Groundwater ferricretes from the Silurian of Ireland and Permian of the Spanish Pyrenees. Sediment Geol. 77, 37–49.